Proceedings of the Combustion Institute 40 (2024) 105651

Contents lists available at ScienceDirect

Proceedings of the Combustion Institute

journal homepage: www.elsevier.com/locate/proci

Cellulose pyrolysis kinetic model: Detailed description of volatile species

Paulo Debiagi [a,b,*,1], Veronica Piazza [c,1], Marco Papagni [d], Alessandra Beretta [c], Alessio Frassoldati [d], Tiziano Faravelli [d]

[a] Nottingham Ningbo China Beacons of Excellence Research and Innovation Institute, University of Nottingham Ningbo China, Ningbo 315100, PR China
[b] Simulation of Reactive Thermo-Fluid Systems (STFS), TU Darmstadt, Otto-Berndt-Strasse 2, 64287 Darmstadt, Germany
[c] Laboratory of Catalysis and Catalytic Processes, Dipartimento di Energia, Politecnico di Milano, Via La Masa 34, Milano 20156, Italy
[d] Department of Chemistry, Materials, and Chemical Engineering, Politecnico di Milano, Piazza Leonardo da Vinci 32, 20133 Milan, Italy

ARTICLE INFO

Keywords:
Kinetic modelling
Cellulose pyrolysis
De-lumping
Detailed volatiles
Product speciation

ABSTRACT

Lignocellulosic biomass is typically composed by a major fraction of cellulose. Its decomposition influences on large extent the biomass rate of pyrolysis and product distribution, affecting process behaviour in thermochemical conversion processes. Containing approximately 90 % of volatile matter, volatile products from cellulose pyrolysis are very important in the characteristics of flames and ignition properties. Recent developments in analytical methods allowed a detailed identification of these volatile products, giving valuable information to process development and better understanding of kinetics. Predictions of a previous kinetic model are compared with these new findings, revealing large space for improvements. In this work, we propose a multi-step kinetic model of cellulose pyrolysis, incorporating the most recent experimental findings into the detailed product description. The model consists of four main reactions for the decomposition of cellulose, with formation of gases, volatiles, char and metaplastic species. The release of metaplastic species is described by a set of six reactions. The formation and release of 13 oxygenated hydrocarbons is predicted by the model, including anhydrosugars, furans, aldehydes, alcohols, ketones and carboxylic acids. The model also describes the formation of levoglucosan in metaplastic state before its release, explaining high heating rate mass loss behaviour. The model is compared with a large variety of experiments from literature, and validated for mass loss rates and product distribution, achieving overall good agreement despite experimental uncertainties and the large simplifications characteristic of the model formulation. Besides effectively quantifying the yields of gaseous, condensable and solid products, the model accurately captures the distribution of volatiles in terms of functional groups and C-chain length.

1. Introduction

Worldwide policies and efforts are supporting the transition in the direction of reaching net-zero emissions in the upcoming decades while effects of the climate crisis become more evident. As of 2020, coal remained the world main energy resource for heat and electricity generation, and the source of more than 40 % of anthropogenic CO2 emissions [1]. Renewable electricity from solar and wind is intermittent, and backup on-demand power will be required in this transition. With 2435 active coal power stations (2.1 TW) in 2023 [2], retrofitting existing infrastructure is a feasible alternative to mitigate emissions maintaining the energy output with minimum capital costs [3].

Using biomass to partially or completely replace coal in power plants is being widely discussed and investigated [4]. When the biomass resource is obtained from waste materials, it does not compete with food supply chain, and also serves as a waste management process [5]. Moreover, when combined with carbon capture technologies, biomass-to-power can reach negative emissions. Waste lignocellulosic biomass is an abundant resource from many agricultural and industrial activities. However, the thermochemical conversion of lignocellulosic biomass is a complex problem that involves multi-scale, multi-phase and multi-component aspects [6,7]. Designing efficient processes for retrofitted combustion chambers requires a deep understanding of these complexities. In this context, the combination of experimental and numerical investigations is a very useful method to unravel the decomposition characteristics and to produce accurate models for the reacting

* Corresponding author.
E-mail address: Paulo.Debiagi@Nottingham.edu.cn (P. Debiagi).
[1] Paulo Debiagi and Veronica Piazza equally contributed to the work.

https://doi.org/10.1016/j.proci.2024.105651
Received 4 December 2023; Accepted 10 July 2024
Available online 19 August 2024

process [8].

Lignocellulosic biomass is typically composed by three major components: cellulose, hemicellulose and lignin. Cellulose accounts for more than 50 % of the dry weight in many feedstocks [9]. The thermochemical conversion of cellulose starts with the devolatilization (pyrolysis), releasing about 90 % of its mass as mixture of light gases and heavier tars, together with formation of minor amounts of solid char. The distribution of these products is strongly influenced by the operating conditions such as heating rate, temperature, particle size and reacting time [7].

Models of the reaction mechanism has been proposed by many authors in the past decades, presenting widely different levels of detail, accuracy and applicability [9]. Among the existing modelling tools which include global kinetic models [10], Distributed Activation Energy Models (DAEM, [11]), network models [12,13] and mechanistic models [14,15], the semi-detailed multistep lumped models represent a compromise between accuracy and flexibility. In this field, the CRECK-S model presents a semi-empirical approach, with intermediate level of complexity and a lumped characterization of products. The model was initially proposed by Faravelli et al. [16], later receiving further improvements regarding product distribution by Ranzi et al. [6,17] and char composition by Debiagi et al. [18]. For these characteristics, this model has been implemented in several research projects, serving as mean to validate experimental data up to reactor designing purposes.

Nevertheless, the model was developed using the literature information available at the time. Recent developments in equipment and analytical methods increased accuracy and resolution of species detected.

In this work, an improved kinetic model for the pyrolysis of cellulose is proposed. The model takes the previously available sub-model of cellulose pyrolysis from the CRECK-S model [18] as a starting point, evaluating its performance. Model refinement is based on newly collected data from the TGA-setup presented in a previous work [19], addressing both devolatilization trends and product distribution. In particular, this novel TGA-based methodology offers accurate experimental data on onset temperatures, released products at specific temperatures and clear effects of heating rates on the pyrolysis process. The scheme is improved by introducing additional species that reflect the new experimental findings, new reactions that account for effects not previously modelled, and calibration of kinetic parameters. The proposed model is further validated with literature data, making sure the general good agreement is still achieved and possibly further improved. For clarity, in this manuscript the published model and the improved model are referred to as Model V20 (year 2020 [18]) and Model V23 (this work), respectively.

The work is organized as follows: the materials and experimental methods are detailed in Section 2, together with a description of Model V20. Section 3 presents a comparison between experimental data collected in TGA-setup and Model V20 predictions, highlighting areas of enhancement. The improvements introduced in Model V23 are explained in Section 4, showing the complete list of lumped species and the lumped kinetic scheme. Then, Section 5 discusses the comparison of TGA data with the refined Model V23, while Section 6 describes the validation of the model with additional literature data and the extrapolation to high heating rate pyrolysis.

2. Materials and methods

2.1. Pyrolysis experiments

A commercial microcrystalline cellulose (Sigma Aldrich, 20 μm) was utilized for this study. The experiments were carried out with a novel TGA-based methodology that allowed to couple the tracking of biomass mass loss curves with a comprehensive quantitative speciation of the entire product slate. Samples of 5–30 mg of powders were used in each experiment and open Pt-pans were employed. The experimental protocol has been presented by the authors in [19], to which the reader is referred for detailed description. Pyrolysis tests were run in a thermogravimetric analyzer (TGA Hitachi STA7300), subjecting cellulose samples to a controlled heating ramp (3–100 K/min) from room temperature to 1073 K, under He flow (85–275 NmL/min). Different analytical techniques and sampling protocols were employed to characterize the diverse classes of pyrolysis products, including solid residual, heavy oxygenates (C_{6+}), light oxygenates (C_1-C_5), gases and H_2O. More specifically, the solid residual was evaluated from mass loss curves measured by the micro-balance. Heavy oxygenates were captured in two in-series commercial sorbing tubes (ORBO™ 609, Supelco) during experiments and integral composition analyses were performed in an offline GC–MS/FID (Agilent 6890, 5973 MSD) to determine the integral mass yields of each species. In contrast, light oxygenates were sampled using a gas syringe during pyrolysis tests (2 mL sample) and offline analyses were performed in the previously described GC–MS/FID; also in this case, the integral mass yield of each species was determined. To conclude, gases and H_2O flowrates were monitored in real-time during pyrolysis tests in an online mass spectrometer (HPR-20 EGA, Hidden Analytical). Calibration protocols were developed to quantitatively determine the integral mass yield of each pyrolysis product; more specifically, calibration factors for online MS were calculated by sending stream with known composition, while fluoronaphthalene was used as internal standard for GC analyses. Reproducibility was controlled by repeating TG experiments, also with varying biomass mass to check for mass transfer limitations. It was observed that devolatilization trends largely coincided, confirming their kinetic relevance, and an apparent activation energy of 41.1 kcal/mol was estimated with a 95 % confidence interval of ± 2.9 kcal/mol. Uncertainties of ±2.0 %, ± 2.7 %, ±1 % and ±2.3 % were estimated for char, levoglucosan, gases and H_2O, respectively. Further details on experimental procedures are found in [19].

Product speciation was evaluated for experiments carried out at the two heating rates of 20 and 100 K/min. The integral productivity of 31 species was determined and mass balances closed to 98.7 % and 100.5 %, respectively.

2.2. CRECK-S cellulose kinetic mechanism

Model V20 [18] describes a single reference species (CELL), which represents the monomer anhydrous-glucose in the polymeric structure of cellulose ($C_6H_{10}O_5$). The thermal decomposition occurs through a first depolymerization step, producing active cellulose ($CELL_a$), which reduces the polymerization degree without release of volatile products. Then, active cellulose may decompose along two competing reactions. One brings to the formation and release of the C_6 anhydrous sugar levoglucosan (LVG), while the second represents the decomposition into H_2O, tars such as hydroxyl-acetaldehyde, glyoxal, propanal, hydroxy-acetone, and 5-hydroxymethylfurfural, lighter products such as formaldehyde, formic acid, CO and CO_2, together with a char residue. The LVG formation path is predominant at temperatures lower than 750 K, while the competing process prevails at higher temperatures due to its higher activation energy. In addition, a side dehydration and charring exothermic reaction directly from CELL is considered, having a higher selectivity at lower temperatures, typical of torrefaction and carbonization processes.

To simulate pyrolysis experiments, this lumped scheme is integrated into a semi-batch reactor model, where the solid biomass undergoes devolatilization and pyrolysis vapours exit the reactor; simulations are performed in OpenSMOKE++, a numerical framework developed by some of the authors for numerical simulations of reacting systems [20]. Heat transfer was considered: for low-heating rate cases, by attributing the experimental TGA temperature program; for high-heating rate cases, by attributing the estimated sample heating rate as reported in the original experimental references.

3. Experimental results and comparison with previous model

Model V20 is used to simulate the experiments in TGA aiming to assess the model predictive accuracy. Fig. 1 compares the measured mass loss trends with model predictions: it is seen that the model well predicts the observed decay and the solid residual, even if with a slight shift at higher temperatures for all the heating ramps. Discrepancies can also be observed in the last 20–30 % of mass loss, mostly at the high heating rates, where the model fails to capture the decrease of reactivity. In contrast, notable limitations emerge in the prediction of product distribution, as illustrated in Fig. 2, where the integral mass yields of different classes of products from cellulose pyrolysis at 100 K/min are shown. Indeed, while the model captures successfully the general trends (e.g. the predominance of levoglucosan, the limited yields of char), a significant discrepancy emerges on underpredictions of C_6 products yields, and overpredictions of light oxygenates and light gases. In particular, the model overpredicts the formation of CO, CO_2, and volatile compounds containing 2 and 3 carbon atoms. Furthermore, the experiments were able to better define the entire range of products with respect to the model; for instance, species C_4, C_5 and C_7 are observed experimentally, but absent in the model. Moreover, experimental results prove a higher yield of anhydrosugars/sugar monomers, while an opposite trend is seen for aliphatic aldehydes/ketones. The enhanced capability of the present experimental configuration to detect and quantify the entire product slate appears of great importance for the refinement of kinetic models of biomass primary devolatilization reactions. To this aim, specific modifications of the CRECK-S model are proposed in the next section.

4. Improvement of the kinetic model

As a result of the new experimental findings, the model was developed including new reactions and new species, as outlined in Table 1. With reference to this kinetic model, species X referred as G{X} represent species adsorbed in metaplastic phase [6].

The framework of new Model V23 is analogous to that of Model V20, involving a first depolymerization step (R1) of a single reference species (CELL), producing active cellulose ($CELL_a$). Notably, in Model V23, this reaction presents a lower activation energy of 45 kcal/mol (compared to 47 kcal/mol in Model V20); this adjustment aims to anticipate the initial devolatilization stage at lower temperatures, in line with the experimental evidence in Fig. 1. Similarly to Model V20, $CELL_a$ may decompose along two parallel reactions: R2, representing the decomposition to anhydrosugars, and R3, the fragmentation to lighter oxygenates, water, CO, CO_2 and char. However, these two reactions are enriched with a partial de-lumping of the species: in particular, a new pseudo-species $C_6H_{10}O_5$ is introduced to account for the production of anhydrosugars that are not levoglucosan, in addition to the predominant LVG. In

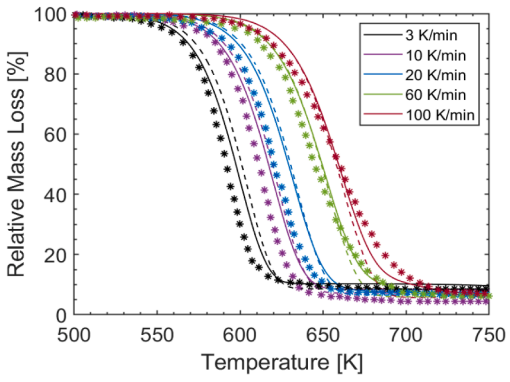

Fig. 1. Mass loss curves at varying heating rates. Scatters = experimental data; dashed lines = Model V20; solid lines = Model V23.

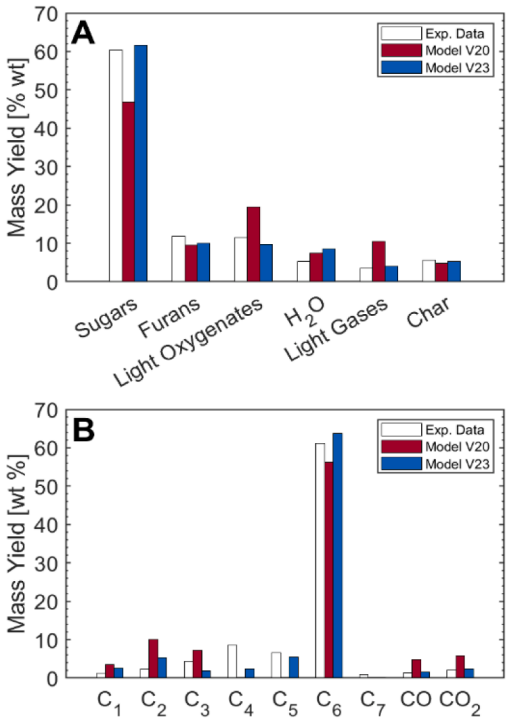

Fig. 2. Product distribution measured from TGA tests at 100 K/min and comparison with model predictions. (A) Sorted by chemical functionalities. (B) Sorted by number of carbon atoms in the molecules.

Table 1
Improved kinetic scheme of cellulose pyrolysis (Model V23).

			Kinetic mechanism	Kinetic parameters A [1 /s], E_{act} [kcal /kmol]
R1	CELL	→	$CELL_a$	$7.00{\cdot}10^{13}{\cdot}exp(-45000/(RT))$
R2	$CELL_a$	→	0.6 LVG+ 0.2 G{LVG} + 0.2 $C_6H_{10}O_5$	$6.92{\cdot}10^{4}{\cdot}exp(-15000/(RT))$
R3	$CELL_a$	→	0.026 CH_2OHCH_2CHO + 0.3705 CH_2OHCHO + 0.036 CHOCHO + 0.049 CH_3CHO + 0.088 $C_6H_6O_3$ + 0.1657 CH_3OH + 0.1058 CH_2O + 0.1595 CO + 0.28 CO_2 + 0.204 H_2 + 1.5007 H_2O + 0.162 HCOOH + 0.0371 CH_4 + 0.901 CHAR + 0.07 G{CO} + 0.05 G $\{COH_2\}_{Loose}$ + 0.024 G{H_2} + 0.18 FURAN + 0.1323 CH_3COCH_3 + 0.287 FURFURAL	$8.50{\cdot}10^{5}{\cdot}exp(-19100/(RT))$
R4	CELL	→	0.125 H_2 + 4.45 H_2O + 5.45 CHAR + 0.125 G{H_2} + 0.12 G$\{COH_2\}_{Stiff}$ + 0.25 G{CO} + 0.18 G $\{COH_2\}_{Loose}$	$8.00{\cdot}10^{7}{\cdot}exp(-31000/(RT))$
R5	G{CO}	→	CO	$5.00{\cdot}10^{12}{\cdot}exp(-52500/(RT))$
R6	G $\{COH_2\}_{Loose}$	→	0.2 CO + 0.2 H_2 + 0.8 H_2O + 0.8 CHAR	$6.00{\cdot}10^{10}{\cdot}exp(-50000/(RT))$
R7	G $\{COH_2\}_{Stiff}$	→	0.8 CO + 0.8 H_2 + 0.2 H_2O + 0.2 CHAR	$1.00{\cdot}10^{9}{\cdot}exp(-59000/(RT))$
R8	G{H_2}	→	H_2	$1.80{\cdot}10^{8}{\cdot}exp(-70000/(RT))$
R9	G{LVG}	→	LVG	$9.50{\cdot}10^{-2}{\cdot}T{\cdot}exp(-10000/(RT))$
R10	G{ LVG}	→	LVG	$6.00{\cdot}10^{11}{\cdot}exp(-45000/(RT))$

contrast, Model V20 used the only pseudo-species LVG for all anhydrosugars. Additionally, metaplastic levoglucosan G{LVG} is introduced to better reproduce the decrease of cellulose reactivity observed within the last 20–30 % of mass loss curves, attributed to its delayed release. To differentiate between low and high temperature behaviors, two release reactions, R9 (lower activation energy) and R10 (higher activation energy), are proposed. Furthermore, additional species FURAN and FURFURAL are introduced among tars produced in R3, representing C_4 and C_5 products, which were absent in Model V20.

In addition to the species de-lumping, guided by the experimental observations, the kinetic parameters of reaction R2 were modified, resulting in a higher R2/R3 ratio and leading to an increase of overall sugar yields at the expense of light oxygenates.

Lastly, a side dehydration and charring exothermic reaction (R4) directly from CELL is considered, similarly to Model V20. Its pre-exponential factor has been increased in order to obtain a larger yield of char.

The complete kinetic mechanism in CHEMKIN format is provided in the Supplementary Material.

5. Comparison of experimental data with updated model

Predictions from modified Model V23 are compared with TGA-data and with previous Model V20 in Figs. 1 and 2, in terms of devolatilization trends and product distribution, respectively. This comparison demonstrates a notable enhancement in model predictions. The reduction in the activation energy of R1 results in a better fit of experimental mass loss curves, anticipating the onset of devolatilization. Additionally, the inclusion of the metaplastic species G{LVG} and its delayed release enables a more accurate description of the high temperature trends. Importantly, there has been a substantial improvement in matching the product distribution: indeed, the change in reactions R2 and R3, and consequently their ratio R2/R3, leads to an increase in sugars yields at the expense of light oxygenates, aligning more closely with experimental observations. Moreover, the partial de-lumping of condensable products significantly improves the description of products. This is better displayed in Fig. 3(A–C), which details mass yields of individual products (both measured products and predicted lumped species), grouped according to their chemical functionality and number of carbon atoms in the molecule. In contrast to the original model, the modified mechanism satisfactorily aligns with experimental data, with furans well distributed in the C_4-C_6 range, and C_1-C_3 light oxygenates; additionally, the new pseudo-species $C_6H_{10}O_5$ well encompasses the sugars that are not LVG. Fig. 3(D) shows the measured and calculated yields of char, gases and LVG at varying heating rates, indicating a good match, with an increase in gases at higher heating rates, and an opposite trend and char. Margins for improvement still remain and deal with the effect of heating rate on levoglucosan yield and the possible introduction of a C_4 lumped species for light oxygenates. Further comparisons are provided in Figs. S1 and S2 in the Supplementary Material (section S.1).

6. Validation of updated model and extrapolation to high heating rates

The validation of the modified Model V23 involves a comprehensive comparison between the model predictions and independent experimental data reported in literature. This validation ensures the reliability and comprehensiveness of the updated cellulose pyrolysis model across a diverse range of experimental conditions and sources.

The initial validation procedure involved an examination on mass

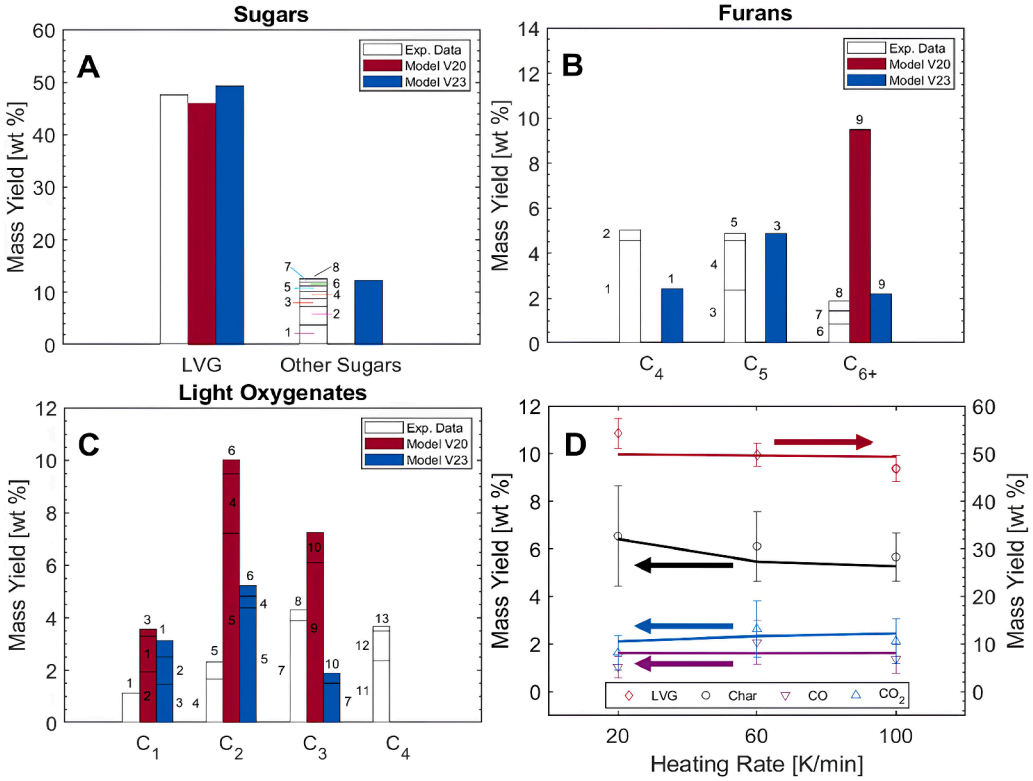

Fig. 3. Details on product distribution from cellulose pyrolysis at 100 K/min: experiments and model predictions. (A) Mass yields of sugars with different C-atoms. (1) AGF, (2) 2-Deoxy-d-galactose, (3) LGO, (4) DGP, (5) 2,3-Anhydro-d-mannosan, (6) d-Allose, (7) 3,4-Anhydro-d-galactosan, (8) DL-arabinose. (B) Mass yields of furans with different C-atoms. (1) Furan, (2) Furan, 2,3-dihydro-, (3) Furfural, (4) 2-methyl-furan, (5) 3-Furaldehyde, (6) Furan, 2-propyl-, (7) Furan, 2,5-dimethyl-, (8) 2-Vinylfuran, (9) Hydroxy-methyl-furfural. (C) Mass yields of light oxygenates with different C-atoms. (1) Formaldehyde, (2) Methanol, (3) Formic Acid, (4) Acetaldehyde, (5) Hydroxy-acetaldehyde, (6) Glyoxal, (7) Acetone, (8) Hydroxy-propanone, (9) Propionaldehyde, (10) Hydroxy-propionaldehyde, (11) Butanedione, (12) Acetic Anhydride, (13) Glutaraldehyde. (D) Mass yields of char, gases and LVG at varying heating rate. Error bars for tests are added.

loss curves, as illustrated in Fig. 4. The comparison was extended across a wide range of heating rates, ranging from slow (10–20 K/min [21]) to fast (10^2–10^3 K/min [22,23]) and extending to flash pyrolysis (10^2 K/s and 10^3 K/s [24]).

Model V23 demonstrates an enhanced agreement with experimental data compared to Model V20; notably, this improved alignment is not confined to the range of slow heating rates considered for model refinement, but it extends convincingly to the extrapolation for fast and flash pyrolysis cases. Indeed, the incorporation of the metaplastic levoglucosan and its delayed release via reactions R9 and R10, improve the predictions of mass loss trends and capture the decrease in reactivity in the final stage of devolatilization, resulting in a significantly more accurate representation of experimental trends. At the highest heating rates, such as the interval 100–1000 K/s, there could be an increased uncertainty between the measured and assumed temperature of the sample, since the experimental dataset was produced a few decades ago. This could explain the apparent discrepancy in the mass loss vs. temperature comparison plot. This discrepancy, on the other hand, is significantly lower when considering the mass loss vs. time comparison (e.g. a difference of 100 K in these comparisons reflects in 1 s (100 K/s) and 0.1 s (1000 K/s) of time discrepancy in the mass loss vs. time). Further comparison of model predictions and experimental mass loss curves from literature studies are shown in Figs. S3 and S4 of the Supplementary Material (section S.2).

The efficacy of the model was then assessed in terms of product distribution. For this analysis, literature data collected in micropyrolyzer experiments were utilized. Indeed, in these setups pyrolysis tests are carried out in precisely controlled condition; a limited amount of biomass (within micrograms to milligrams range) undergoes extremely rapid heating (up to 10^4 K/s) and primary devolatilization products are quickly removed from the reacting zone to prevent the onset of secondary reactions. Therefore, micropyrolyzers offer an important advantage for the kinetic investigation, with respect to traditional fixed bed tests that can be affected by heat and mass transfer limitations, and where biomass heating is not trivial. Moreover, the comparison of Model V23 predictions with micropyrolyzer outcomes allows to test the efficacy of the model within heating rates that are consistently higher than those explored in TGA. Instead, the scarcity of complete speciation data from TGA experiments in the existing literature limits the model validation at low heating rates in terms of speciation.

A dataset of isothermal experiments carried out in micropyrolyzer on diverse commercial celluloses (microcrystalline and non-microcrystalline) and covering a temperature range of 673K-873 K was utilized for model assessment [15,25–30]. Measured and predicted mass yields of different categories of products - LVG, furans, light oxygenates and light gases - were compared, as shown in Fig. 5. An extended version is shown in Fig. S5 in the Supplementary Material (section S.3) where mass yields of H_2O and char are also displayed. Notably, there is visible variance among experimental data; therefore, the model aims to find a balance in its predictions. Fig. 5(A) demonstrates an improvement in predictive capability of Model V23 for the production of LVG, with refined LVG yields higher than those of Model V20 (e.g., at 773K: 42.8 % for Model V23 vs 27.48 % for Model V20). Although the refined model better aligns with the experimental data, it still tends to underestimate LVG production (e.g. the majority of the experiments lie between 55 and 70 % at 773 K). Evaluating the discrepancies between the model and the measurements, it has to be considered that often no uncertainties are discussed for the experimental data. Moreover, the lumped approach of the model does not allow to increase the agreement with these data, without losing the accuracy in reproducing the most recent data [19]. Fig. 5(B) reports the measured and calculated mass yields of furans at different temperatures: in this case, Model V23 differs slightly from the previous version, and both models overestimate furans production. This evidence, coupled with the insights from LVG, suggests that pyrolysis at high heating rates (i.e. high temperature) tends to form less furans and more sugars compared to low heating rates in TGA. Fig. 5(C) demonstrates that the Model V23 predictions agree with the experimental mass yields of light oxygenates for the majority of data Fig. 5(D) shows a significant improvement in the predictions of light gases (mainly CO and CO_2) in Model V23, while they were previously overvalued. Lastly, also predictions of H_2O and char well aligns with experimental trends (Figs. S5 and S6).

To visualise the effect of species de-lumping in Model V23, a more detailed comparison is shown for two set of experiments at 773 K, from Zhou et al. [25] and Patwardhan et al. [29]. Condensable volatiles were grouped according to their C-chain length, and gas species CO and CO_2 were individually analysed. The comparison between experimental measurements and model predictions shown in Fig. 6 highlights a significant improvement in the level of detail achieved in Model V23 description. In both cases, the updated model accurately captures the yields of CO and CO_2, which were instead greatly overestimated by Model V20. Moreover, while the impact on char and H_2O remained almost unchanged (as discussed for Fig. 5), Model V23 significantly improves the depiction of volatiles distribution across the C_1-C_6 range. In particular, yields of C_6 species (mainly LVG, but also other anhydrosugars and hydroxy-methyl furfural) are increased in Model V23 and better align experimental results. Conversely, the yield of light oxygenates in the C_1-C_3 range is diminished, reflecting experimental evidence. Additionally, the inclusion of C_4 of C_5 lumped species allows for a better depiction of the results from Patwardhan et al. (Fig. 6(A)); instead, these species were not detected by Zhou et al. (Fig. 6(B)).

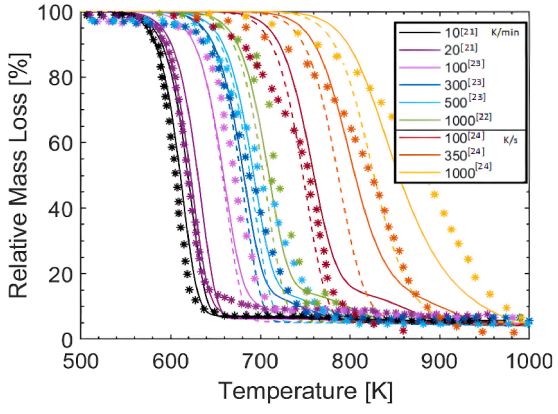

Fig. 4. Mass loss curves at varying heating rates. Scatters = experimental data [21-24]; dashed lines = Model V20; solid lines = Model V23.

7. Conclusions

This work presents an updated lumped kinetic scheme of cellulose pyrolysis, refined by an accurate description of volatile speciation. The development of the model is based on novel experimental data collected in a TGA-setup, that couples mass loss trends monitoring with a comprehensive speciation of pyrolysis products. The refined model consists in ten lumped reactions and includes the formation and the release of 13 oxygenated volatiles (anhydrosugars, furans, aldehydes, alcohols, ketones and carboxylic acids), as well as light gases and water. Model predictions are compared with literature data collected in micropyrolyzers, both serving as model validation and demonstrating a good accuracy in describing a wide range of heating rates. The model successfully captures mass loss trends for slow (3 K/min), fast (10^3 K /min) and flash pyrolysis (10^3 K/s), and stands out for its good ability to predict both the yields and the distribution of volatiles, well capturing the ratio between C_6 sugars and light oxygenates resulting from further fragmentation of cellulose chain. The partial de-lumping of species enhances model descriptive capacity in terms of C_6 anhydrosugars, C_4-C_6 furans and C_1-C_3 light oxygenates, without compromising model

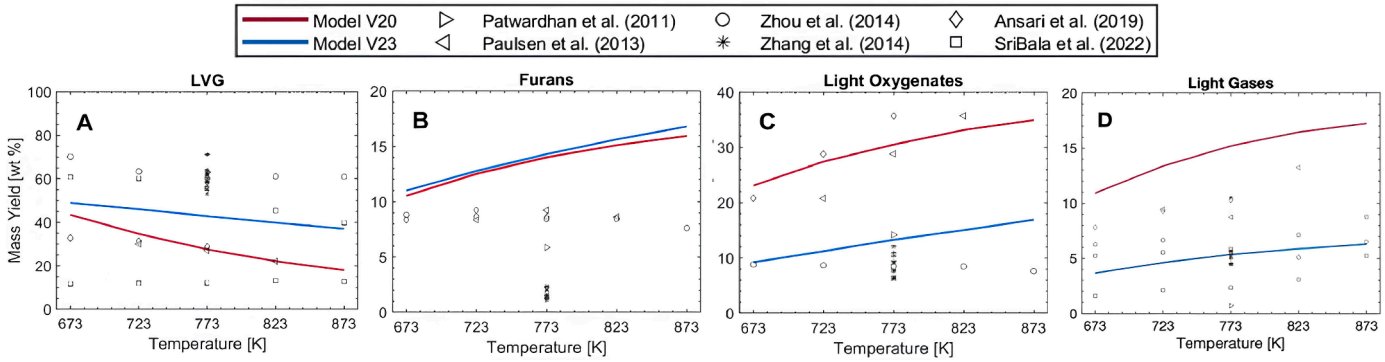

Fig. 5. Comparison between model predictions and experimental data from the literature in terms of mass yields: (A) LVG, (B) Furans, (C) Light Oxygenates, (D) Light Gases. [15,25-30].

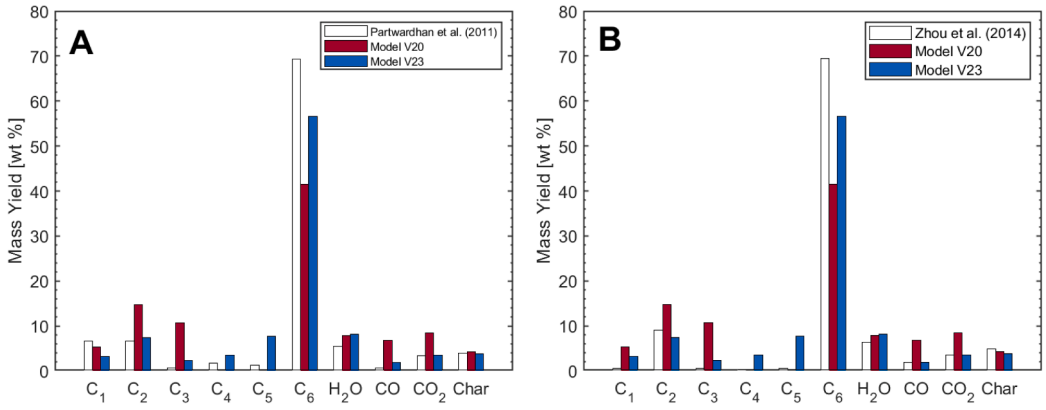

Fig. 6. Comparison between model predictions and experimental data from literature at 773 K: detailed speciation [25,29].

flexibility. The proposed model emerges as a flexible and effective modelling tool for technology optimization, offering valuable insights for the advancement of cellulose pyrolysis processes.

Novelty and significance statement

The novelty of this research is a novel kinetic model for cellulose pyrolysis, advancing the level of details on the volatile species description and additional reacting paths, describing a delayed release of entrapped levoglucosan. It is significant because advancements in analytical measurements allowed an increase in experimental data resolution, revealing new details in primary pyrolysis products. These advancements on the experimental side require an equivalent improvement on the modelling side, incorporating new findings. The proposed model accounts for thirteen oxygenated hydrocarbons distributed among sugars, furans, and light oxygenated products. This level of detail is important for thermochemical conversion processes, as the properties and the amounts of these volatiles directly influence mixture flammability, ignition delay time, flame speed and temperature. The relevance of this model is also reflected on its ideal balance of complexity, offering a predictive and CPU-affordable chemical kinetic model for numerical investigations of reactive systems including CFD simulations.

Author contributions

- PD conceptualization, model development, writing, reviewing
- VP conceptualization, experiments, writing, reviewing
- MP model development, writing
- AB supervision, conceptualization, reviewing
- AF supervision, conceptualization, reviewing
- TF supervision, conceptualization, reviewing

Declaration of competing interest

The authors declare that they have no known competing financial interests or personal relationships that could have appeared to influence the work reported in this paper.

Acknowledgements

PD acknowledges the DFG - German Research Foundation for financial support (project number 215035359 - CRC 129). TF acknowledges that this study was carried out within the NEST - Network 4 Energy Sustainable Transition (D.D. 1243 02/08/2022, PE00000021) and received funding under the National Recovery and Resilience Plan, Mission 4 Component 2 Investment 1.3, funded from NextGenerationEU. This study was partially conducted within the Agritech National Research Center and received funding from the EU NextGenerationEU (PNRR) – MISSIONE 4 COMPONENTE 2, INVESTIMENTO 1.4 and 1.3 – D.D. 1032 17/06/2022, CN00000022). This work reflects only the authors' views and opinions, neither European Union nor European Commission are responsible for them.

Supplementary materials

Supplementary material associated with this article can be found, in the online version, at doi:10.1016/j.proci.2024.105651.

References

[1] International Energy Agency Electricity generation by source (2021) (accessed: October 2023).

[2] Global Energy Monitor S. Global coal plant tracker (2023) (accessed: October 2023).

[3] J. Janicka, P. Debiagi, A. Scholtissek, A. Dreizler, B. Epple, R. Pawellek, A. Maltsev, C. Hasse, The potential of retrofitting existing coal power plants: a case study for operation with green iron, Appl. Energy 339 (2023), https://doi.org/10.1016/j.apenergy.2023.120950.

[4] F. Sher, A. Yaqoob, F. Saeed, S. Zhang, Z. Jahan, J.J. Klemeš, Torrefied biomass fuels as a renewable alternative to coal in co-firing for power generation, Energy 209 (2020), https://doi.org/10.1016/j.energy.2020.118444.

[5] J.M. Aberilla, A. Gallego-Schmid, A. Azapagic, Environmental sustainability of small-scale biomass power technologies for agricultural communities in developing countries, Renew. Energy 141 (2019) 493–506, https://doi.org/10.1016/j.renene.2019.04.036.

[6] E. Ranzi, P.E.A. Debiagi, A. Frassoldati, Mathematical modeling of fast biomass pyrolysis and bio-oil formation. note I: kinetic mechanism of biomass pyrolysis, ACS Sustain. Chem. Eng. 5 (2017) 2867–2881, https://doi.org/10.1021/acssuschemeng.6b03096.

[7] E. Ranzi, P.E.A. Debiagi, A. Frassoldati, Mathematical modeling of fast biomass pyrolysis and bio-oil formation. note II: secondary gas-phase reactions and bio-oil formation, ACS Sustain. Chem. Eng. 5 (2017) 2882–2896, https://doi.org/10.1021/acssuschemeng.6b03098.

[8] P. Debiagi, C. Ontyd, S. Pielsticker, M. Schiemann, T. Faravelli, R. Kneer, C. Hasse, V. Scherer, Calibration and validation of a comprehensive kinetic model of coal conversion in inert, air and oxy-fuel conditions using data from multiple test rigs, Fuel 290 (2021), https://doi.org/10.1016/j.fuel.2020.119682.

[9] S. Wang, G. Dai, H. Yang, Z. Luo, Lignocellulosic biomass pyrolysis mechanism: a state-of-the-art review, Prog. Energy Combust. Sci. 62 (2017) 33–86, https://doi.org/10.1016/j.pecs.2017.05.004.

[10] J. Kristanto, A.F. Daniyal, D.Y. Pratama, I.N.M. Bening, L. Setiawan, M.M. Azis, S. Purwono, Kinetic study on the slow pyrolysis of isolated cellulose and lignin from teak sawdust, Thermochim. Acta 711 (2022), https://doi.org/10.1016/j.tca.2022.179202.

[11] T. Sonobe, N. Worasuwannarak, Kinetic analyses of biomass pyrolysis using the distributed activation energy model, Fuel 87 (2008) 414–421, https://doi.org/10.1016/j.fuel.2007.05.004.

[12] S. Hameed, A. Sharma, V. Pareek, H. Wu, Y. Yu, A review on biomass pyrolysis models: kinetic, network and mechanistic models, Biomass Bioenergy 123 (2019) 104–122, https://doi.org/10.1016/j.biombioe.2019.02.008.

[13] A.D. Lewis, T.H. Fletcher, Prediction of sawdust pyrolysis yields from a flat-flame burner using the CPD model, Energy Fuel. 27 (2013) 942–953, https://doi.org/10.1021/ef3018783.

[14] R. Vinu, L.J. Broadbelt, A mechanistic model of fast pyrolysis of glucose-based carbohydrates to predict bio-oil composition, Energy Environ. Sci. 5 (2012) 9808–9826, https://doi.org/10.1039/c2ee22784c.

[15] X. Zhou, M.W. Nolte, B.H. Shanks, L.J. Broadbelt, Experimental and mechanistic modeling of fast pyrolysis of neat glucose-based carbohydrates. 2. validation and evaluation of the mechanistic model, Ind. Eng. Chem. Res. 53 (2014) 13290–13301, https://doi.org/10.1021/ie502259w.

[16] T. Faravelli, Multistep kinetic model of biomass pyrolysis, Green Energy Technol. (2003) 447–466, https://doi.org/10.1007/978-1-4471-5307-8.

[17] E. Ranzi, M. Corbetta, F. Manenti, S. Pierucci, Kinetic modeling of the thermal degradation and combustion of biomass, Chem. Eng. Sci. 110 (2014) 2–12, https://doi.org/10.1016/j.ces.2013.08.014.

[18] P. Debiagi, G. Gentile, A. Cuoci, A. Frassoldati, E. Ranzi, T. Faravelli, A predictive model of biochar formation and characterization, J. Anal. Appl. Pyroly. 134 (2018) 326–335, https://doi.org/10.1016/j.jaap.2018.06.022.

[19] V. Piazza, R. Da Silva JR, A. Frassoldati, L. Lietti, S. Chiaberge, C. Gambaro, A. Siviero, T. Faravelli, A. Beretta, Detailed speciation of biomass pyrolysis products with a novel TGA-based methodology: the case-study of cellulose, J. Anal. Appl. Pyroly. 178 (2024) 106413, https://doi.org/10.1016/j.jaap.2024.106413.

[20] A. Cuoci, A. Frassoldati, T. Faravelli, E. Ranzi, OpenSMOKE++: an object-oriented framework for the numerical modeling of reactive systems with detailed kinetic mechanisms, Comput. Phys. Commun. 192 (2015) 237–264, https://doi.org/10.1016/j.cpc.2015.02.014.

[21] Z. Gao, N. Li, M. Chen, W. Yi, Comparative study on the pyrolysis of cellulose and its model compounds, Fuel Process. Technol. 193 (2019) 131–140, https://doi.org/10.1016/j.fuproc.2019.04.038.

[22] Y. Qiao, B. Wang, Y. Ji, F. Xu, P. Zong, J. Zhang, Y. Tian, Thermal decomposition of castor oil, corn starch, soy protein, lignin, xylan, and cellulose during fast pyrolysis, Bioresour. Technol. 278 (2019) 287–295, https://doi.org/10.1016/j.biortech.2019.01.102.

[23] I. Milosavljevic, E.M. Suuberg, Cellulose thermal decomposition kinetics: global mass loss kinetics, Ind. Eng. Chem. Res. 34 (1995) 1081–1091, https://doi.org/10.1021/ie00043a009.

[24] M.R. Hajaligol, J.B. Howard, J.P. Longwell, W.A. Peters, Product compositions and kinetics for rapid pyrolysis of cellulose, Ind. Eng. Chem. Process Des. Dev 21 (1982) 457–465. https://pubs.acs.org/sharingguidelines.

[25] X. Zhou, M.W. Nolte, H.B. Mayes, B.H. Shanks, L.J. Broadbelt, Experimental and mechanistic modeling of fast pyrolysis of neat glucose-based carbohydrates. 1. Experiments and development of a detailed mechanistic model, Ind. Eng. Chem. Res. 53 (2014) 13274–13289, https://doi.org/10.1021/ie502259w.

[26] A.D. Paulsen, M.S. Mettler, P.J. Dauenhauer, The role of sample dimension and temperature in cellulose pyrolysis, Energy Fuel. (2013) 2126–2134, https://doi.org/10.1021/ef302117j.

[27] K.B. Ansari, J.S. Arora, J.W. Chew, P.J. Dauenhauer, S.H. Mushrif, Fast pyrolysis of cellulose, hemicellulose, and lignin: effect of operating temperature on bio-oil yield and composition and insights into the intrinsic pyrolysis chemistry, Ind. Eng. Chem. Res. 58 (2019) 15838–15852, https://doi.org/10.1021/acs.iecr.9b00920.

[28] G. SriBala, D.C. Vargas, P. Kostetskyy, R. Van de Vijver, L.J. Broadbelt, G.B. Marin, K.M. Van Geem, New perspectives into cellulose fast pyrolysis kinetics using a Py-GC × GC-FID/MS system, ACS Eng. Au 2 (2022) 320–332, https://doi.org/10.1021/acsengineeringau.2c00006.

[29] P.R. Patwardhan, D.L. Dalluge, B.H. Shanks, R.C. Brown, Distinguishing primary and secondary reactions of cellulose pyrolysis, Bioresour. Technol. 102 (2011) 5265–5269, https://doi.org/10.1016/j.biortech.2011.02.018.

[30] J. Zhang, M.W. Nolte, B.H. Shanks, Investigation of primary reactions and secondary effects from the pyrolysis of different celluloses, ACS Sustain. Chem. Eng. 2 (2014) 2820–2830, https://doi.org/10.1021/sc500592v.